

# Toward Computing Cross-Modality Symmetric Non-Rigid Medical Image Registration

SNIGDHA MOHANTY<sup>1</sup> AND SARADA PRASAD DAKUA<sup>1,2</sup>, (Member, IEEE)

<sup>1</sup>School of Electronics, KIIT University, Bhubaneswar 751024, India

<sup>2</sup>Department of Surgery, Hamad Medical Corporation, Doha, Qatar

Corresponding author: Sarada Prasad Dakua (sdakua@hamad.qa)

This publication was made possible by NPRP- 11S-1219-170106 from the Qatar National Research Fund (a member of Qatar Foundation). The findings herein reflect the work, and are solely the responsibility of the authors. The Open Access funding was provided by Qatar National Library.

**ABSTRACT** This paper describes a new non-rigid approach to register images from same- and cross-imaging modalities such as magnetic resonance imaging, computed tomography, and 3D rotational angiography. The deformation is a key challenge in medical image registration. We have proposed a diffeomorphism-based method to tackle this problem using an optimized framework. A non stationary velocity field is used to minimize the effect of forces that are derived from the image gradients. Furthermore, we propose a similarity energy function, based on the gray scale distribution, to limit the fluctuations while approaching the local minima. The proposed method is evaluated on both private and public datasets; the results show that the values of mean square error (MSE), normalized cross-correlation (NCC), structural similarity (SS), mutual information (MI), feature similarity index (FSIM), and mean absolute error (MAE) are 1.3136, 0.9962, 0.9897, 0.883, 0.9922, and  $1.52 \pm 2.09$ , respectively. Both qualitative and quantitative evaluation show promising registration accuracy reflecting the potential of the proposed method.

**INDEX TERMS** Image registration, diffeomorphism, MRI, CT.

## I. INTRODUCTION

There are different types of imaging modalities such as computed tomography (CT), ultrasound imaging (US), three dimensional rotational angiography (3DRA), and magnetic resonance imaging (MRI) that have been used by the clinicians to diagnose, plan and treat the health issue [1], [2]. The patient's real world coordinate must be registered with this data to keep both data and patient in the same perspective; this helps the clinicians to quickly and appropriately plan. The image registration finds the optimal transformation that best aligns the structures of interest in the input images.

### A. CLINICAL USES OF MULTI-MODAL REGISTRATION AND CHALLENGES

Multi-modal registration is important in medical imaging, remote sensing, and cross-modal learning (Fig. 1). Specifically, the deformable registration of MRI and CT images finds clinically relevant applications that include treatment planning, computer-aided diagnosis, multimodal diagnostics, surgery simulation [3], radiotherapy [4],


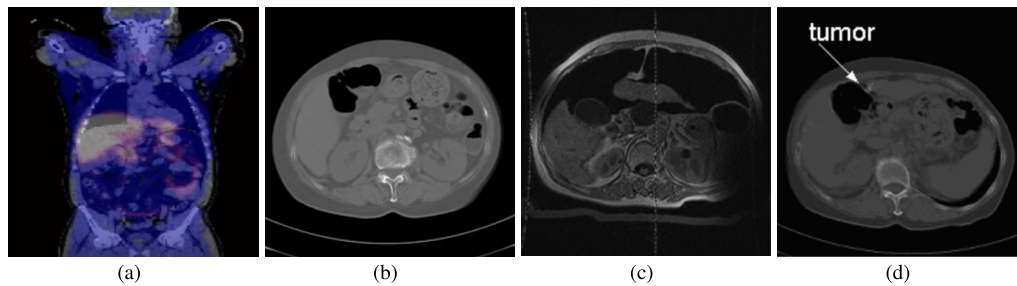
The associate editor coordinating the review of this manuscript and approving it for publication was Easter Selvan Suvisheshamuthu .

image-guided interventions, assisted/guided surgery [5], and disease follow-up. In interventional radiology, the pre-operative CT can be registered with intra-operative US images for hepatobiliary procedures to better visualize the lesions spread across the liver. Same-modal registration is complicated due to motion or disease progression, whereas multi-modal fusion is further challenging mainly due to: 1- non-functional intensity mapping across MRI and CT, 2- locally varying contrast patterns along with others.

### B. RELATED WORK

A number of multimodal medical image registration methodologies have been reported over the years [6]- [14]. Turco *et al.* [15] present the impact of positron emission tomography (PET)/CT attenuation correction on the registration between cardiac PET and a CT image. It is found that blurring introduced by the heart beating has negligible effect on the registration, however, the noise has adverse impact on the registration outcome. Pilutti *et al.* [16] propose a Non-Parametric Bayesian Registration that assumes model for the effect of distortions caused by heartbeat and peristalsis; here, a Gaussian filtering is applied for spatial regularization towards deriving the MR image registration.



**FIGURE 1.** Visualizing the liver anatomy and illustrating multi-modal (CT and MR) image registration to identify a tumour.

Wang *et al.* propose a model-to-surface MR/US registration with the help of statistical deformable model and finite element analysis to establish the surface-point correspondence. Samei *et al.* [17] present a finite element-based registration method of 3D to 2.5D transrectal US images, where the method relies on the outcome of an intermediate step to extract arbitrary slices from a 3D image. Cao *et al.* [18] propose a region-adaptive CT/MRI registration method with the help of multi-target regression forest to deal with the large appearance gaps. Zhou *et al.* [20] present a framework based on correlation-weighted sparse representation in order to separate the contrast agent from the input dynamic contrast-enhanced (DCE)-MR images allowing the motion components to be effectively registered. Xu *et al.* [19] present a method for MR/CT registration that co-registers pre-operative MR image with intra-operative binary CT image using a rigid approach to make it faster; subsequently, non-rigid approach is used to correct tiny misalignments.

In recent years, machine learning (ML) and deep learning (DL) have vigorously gained traction in medical image registration. Huang *et al.* [21] present an unsupervised learning-based framework, where the network consists of affine and deformable transformations. Hansen *et al.* [22] propose a sparse key point-based geometric network that leverages discrete dense displacement maps facilitating the registration process. Grim *et al.* [23] present a method that first trains a neural network to detect a set of anatomical landmarks, then, the combination of landmark locations and network is used in computing the initializations to incorporate the confidence of the network to detect the landmarks. Yu *et al.* [24] present an unsupervised network based on a metabolic constraint function and a multi-domain similarity measure towards determining PET/CT registration that uses standard uptake value (SUV) distribution of hypermetabolic regions of the human organs or region of interest (ROI). Fechter and Baltas [25] employ a method that combines U-Net with a coarse-to-fine approach and a differential spatial transformer module to estimate deformable image registration. Guan *et al.* [26] present a multi-channel convolutional neural network that combines a periodic vascular diameter variation model with the convolutional neural network (CNN) registering digital subtraction angiography images with their 3D models. Thus, the literature shows that the research

fraternity has shown more inclination towards these ML/DL-based methods, however, there have been several limitations that still remain unanswered: Deep learning (DL)-based methods, specifically neural networks for medical image registration, have received attention due to their end-to-end nature and state-of-the-art performance. However, neural networks face several challenges that are not present in the conventional methods [45]. In a clinical setting, these variations are expected in the data due to multiple machines with several acquisition parameters that can cause the data distribution to change. One technical limitation for training the neural networks is due to the limited quantity of clinical data, resulting in overfitting (i.e., poor generalizability). Additionally, the training procedure of the neural networks does not provide any convergence guarantees. Other technical challenges include the black-box nature of deep learning-based approaches, which downplays the reliability of the neural networks in clinically sensitive settings [46].

We realize the above mentioned issues, especially, the shortage of clinical data and thus decided to focus on the conventional methods. Yipeng *et al.* [27] present a method for generating a subject-specific statistical shape model capturing the prostate deformation. Li *et al.* [28] introduce an objective function for similarity measurement that embeds the local phase features derived from monogenic signal in the modality independent neighborhood descriptor based on autocorrelation of local structure. Pai *et al.* [30] propose a multi-scale, multi-kernel shape, compactly supported kernel bundle framework for stationary velocity field-based image registration. Jarrod *et al.* [32] describe a human-to-phantom validation framework that transforms the surface collection patterns from *in vivo* image-guided liver surgery procedures onto a well-characterized hepatic deformation phantom for validating surface-driven nonrigid registration. Sun *et al.* [33] use lower-order B-spline functions for registration, while preserving smoothness of the deformation. Chakraborty *et al.* [36] propose a 2D myocardial deformation imaging to develop a nonrigid image registration motion estimator adapted to radio frequency (RF) data sets. Darkner *et al.* [37] present collocation for diffeomorphic deformations as a numerical solution to diffeomorphic image registration using an implicit A-stable collocation method. Qin *et al.* [40] combine two separate

methods: 1- a superpixel-based structure scale estimator to estimate the boundary-aware structure scale of each reference structure, 2- an edge-aware mismatch scale measuring the mismatch degree of the edge structures to be matched in the images. Sureerat *et al.* [31] present a symmetric diffeomorphic deformable registration algorithm incorporating a modality-independent neighborhood descriptor and a Huber metric for MR/CT registration. Zhang *et al.* [41] use local-phase mean and phase-congruency values of different orientations, to improve the robustness and accuracy using filter-bank of Log-Gabor filters at different orientations and frequencies. Yang *et al.* [42] use an adaptive weighted objective function that formulates the alignment of two point sets as a mixture model estimation problem.

Despite having rich literature, the problems are many and they still remain: 1) different physical acquisition processes may generate statistical correlation between imaging structures that do not correspond to the same anatomical structures, violating one of the underlying assumptions for most intensity-based similarity measures, and 2) the deformation, spatial and temporal variabilities. The ability to capture the complex image deformations and establish accurate point-wise correspondence is key to many computer vision applications that involve image registration and atlas construction. These properties become particularly challenging, when the object depicted on the images undergoes a severe deformation or has a high shape variability. Dissimilarities can occur due to inter- and intra-fractional anatomical variations from the pre-operative image set, i.e. variations between different treatment sessions and during single treatment sessions, respectively. Furthermore, the imaging data is taken from different imaging devices (multi-modality) and may be taken within different time frames (multi-temporality). Deformable registration has a significantly greater number of degrees of freedom (DOF) to manage the aforementioned local distortions between anatomical structures. Interestingly, diffeomorphism methods [30], [31], [37], [41] register images slowly warp images until a satisfying overlap is attained; this method is particularly capable of preventing an invalid folding of the deformation field and guarantees a smooth one-to-one mapping between points. However, these registration methods have been domain specific and parameter sensitive. The update scheme relies on forces derived from the image gradients (even though partially) and is therefore fundamentally limited by the local scope. Therefore, we have proposed a new diffeomorphism-based method that designs a similarity energy function overcoming these problems.

The rest of the paper is organized as follows: Section II describes the clinical data used and the proposed method, Section III includes the results obtained by the method. Finally, Section V concludes the paper.

## II. DATA AND METHODOLOGY

### A. DATA

We have used both private (Hamad Medical Corporation) and publicly available datasets. The data that have been

obtained from Hamad Medical Corporation have the following description: each dataset consists of 700 slices acquired along the long axes of the subjects. The average slice thickness, pixel spacing, and matrix size are 0.29 mm, 0.29 mm $\times$ 0.29 mm, and 512 $\times$ 512, respectively. In the public dataset [43], and [44], a single inversion pulse is followed by a 400 ms delay time. As a result magnetization-prepared 180 degrees radio-frequency pulses and rapid gradient-echo (MP-RAGE) images are T1-weighted. The excitation pulse has a 10 degree flip angle, echo time (TE) is 4 ms, and TR is 10 ms. The resolution is 128  $\times$  256 $\times$ 256. The ground truth data were provided by the respective organizations.

### B. METHODOLOGY

Generally, an image registration aims at determining the spatial correspondence of two or more image sets for minimizing their differences. Let us consider two image sets: a static,  $Fxd$ , and a dynamic/moving,  $Mvg$ ; image registration algorithms try to find the optimal transform minimizing the difference between  $Fxd$  and  $Mvg$ . Such algorithms can be rigid or deformable. For rigid image registration, the translation and rotation of all image pixels is uniform, such that all pixel-to-pixel relationships within the image set remain equal before and after the transformation. For deformable registration (also called non-rigid), those pixel-to-pixel relationships change, i.e., while two image sets are aligned on the same reference coordinate, a pixel in each image set on the same coordinate may not necessarily represent the same anatomical structure. Therefore, deformable image registration can account for local distortions, occurring since organs and tissues are non-rigid structures and subject to deformation. In our method, we use the nearest-neighbor searches establishing the global correspondences between the images; the spectral forces capture the substantial deformations. This is a diffeomorphism-based method that uses an optimized framework venturing the global scope and the speed of nearest-neighbor search to limit/capture the deformations. The theory of Lie groups states that a diffeomorphic transformation  $\phi$  resides in a Lie structure [37]. Furthermore,  $\phi$  is associated with velocity field by,  $\phi = e^v$ . However, in case of stationary velocity fields,  $\phi = e^v$  [29], where  $v$  is the velocity field and  $\phi$  is the diffeomorphism. In this work, we perform feature matching followed by the spectral representations. Section II-B1 describes the similarity metric used for symmetric registration, Section II-B2 discusses the velocity field inducing diffeomorphic mapping. The working flow-chart of the method is provided in Fig. 2.

#### 1) SIMILARITY METRIC FOR SYMMETRIC REGISTRATION

Intensity-based measures are divided into statistical measures, information theoretic measures, and measures that consider the dependency of neighboring pixels [34], [35], [38]. Pearson correlation coefficient, Spearman correlation coefficient, mean square differences, and Hellinger distance are some of the statistical measures. Similarly, there are other methods in information theoretic measures

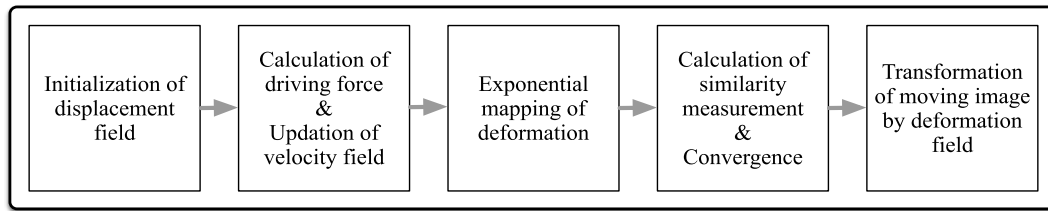


FIGURE 2. The block diagram of the proposed methodology highlighting the key stages of the registration process.

such as mutual information, entropy correlation coefficient, and Kullback-Leibler distance. Furthermore, there are also approaches in spatial dependency measures such as second order mutual information, gradient mutual information, etc. The registration is sort of a matching, where the feature vectors  $Fxd$  and  $Mvg$  are matched via the correspondence map. The feature vectors include the image intensity and spatial information:  $Fxd = (\alpha_i I_{Fxd}, \alpha_s x_{Fxd})$  and  $Mvg = (\alpha_i I_{Mvg}, \alpha_s x_{Mvg})$ , where  $I(\cdot)$  is a pixel intensity and  $x(\cdot) = (x, y)$  is a point coordinate, both weighted with parameters  $\alpha_{i,s}$ . Since we only consider diffeomorphic deformations, in such deformation, the inverse of a mapping exists and is continuously differentiable, that means  $\|x - (\psi \circ \phi)\| \approx 0$  and  $\psi = \phi^{-1}$  such that  $Id = \psi \circ \phi$ , where  $\phi$  is the transformation mapping the points from  $Mvg$  to  $Fxd$  and  $\phi$  is that from  $Fxd$  to  $Mvg$ . It may be noted that  $\circ$  denotes the the composition of functions. In this work, we intend to register two images ( $Fxd, Mvg$ ) either from same modality, where the images have been acquired at different time instants or from different modalities;  $Fxd, Mvg : \Omega \rightarrow \Gamma$ , where  $\Omega \subseteq \mathbb{R}^N$  is the image domain and  $\Gamma \subseteq \mathbb{R}$  is the value domain. The aim is to seek a bijective mapping  $\phi : \Omega \rightarrow \Omega$  such that  $Fxd \circ \phi$  improves the similarity to  $Mvg$  and  $Mvg \circ \phi^{-1}$  improves similarity to  $Fxd$  under the similarity metric or function:

$$\begin{aligned}
 En(\phi) &= Sim(Fxd, Mvg \circ \phi) \\
 &= \frac{1}{2} \|Fxd - Mvg \circ \phi\|^2 + \frac{1}{\lambda_\phi} Reg(\phi) \\
 &= \frac{1}{2|\Omega_p|} \sum_{p \in \Omega_p} |Fxd(p) - Mvg(\phi(p))| \\
 &\quad + \frac{1}{\lambda_\phi} Reg(\phi) \quad (1)
 \end{aligned}$$

where  $p, \circ, Reg, \lambda_\phi, \Omega$ , represent the mapping of pixel, transformation operator, regularization term, regularization parameter, and common region of two input images  $Fxd$  and  $Mvg$  after registration, respectively [50];  $\lambda_\phi = \frac{\alpha_i^2}{\alpha_s^2}$  and  $Reg(\phi) = \|x_{Fxd} - x_{Mvg \circ \phi}\|$ .

In order to minimize, a hidden variable is introduced that considers the regularization criterion as a prior on the smoothness of the transformation  $\phi$ . Instead of requiring the point correspondences between the image pixels (a vector field  $l$ ) to be the exact of the transformation, some error is introduced at each image point. Thus, we introduce a non-ruled spatial transform parameter  $l$ , that makes the new

symmetric function as:

$$\begin{aligned}
 En(l, \phi) &= \|(Fxd - Mvg \circ l)\|^2 \\
 &\quad + \frac{1}{\lambda_{un}^2} Dist(l, \phi)^2 + \frac{1}{\lambda_\phi} Reg(\phi) \quad (2)
 \end{aligned}$$

where  $Dist(l, \phi) = \|l - \phi\|$ ,  $\lambda_{un}^2$  represent uncertainty degree between  $l$  and  $\phi$ , respectively. The displacement field  $u$  is produced using the space geometric transform, and two vectors are added directly to form a new vector. The energy functional then becomes:

$$En(u) = \frac{1}{2} \|Fxd - Mvg \circ (\phi + u)\|^2 + \frac{1}{\lambda_{un}^2} \|u\|^2 \quad (3)$$

where  $\|u\| = \|l - \phi\|$ . The energy function depends on two fields,  $l$  and  $\phi$ , thus it is minimized with respect to  $l$  and  $\phi$ . We first start with  $\phi_0 = Id$  at iteration 0; then iteratively at iteration= $n, 1$ ) we find  $l_n$  by minimizing  $\frac{1}{2} \|Fxd - Mvg \circ (l)\|^2 + \frac{1}{\lambda_{un}^2} \|l_n - \phi_{n-1}\|^2$  using gradient descent method [58], 2) we find  $\phi_n$ , minimizing  $\frac{1}{2} \|Fxd - Mvg \circ (l)\|^2 + \frac{1}{\lambda_{un}^2} \|l_n - \phi_n\|^2$  using single convolution [59]. After minimizing the energy function and solving the displacement field, the final displacement field is obtained. Diffeomorphic transform or space ensures reversible, smooth deformation and topologically invariant deformation.

## 2) VELOCITY FIELD INDUCING DIFFEOMORPHIC MAPPING

Since there is deformation, we consider a non-stationary velocity field (nSVF), where the initial velocity (or equivalently the momentum map) is different at different time points along a geodesic [49]. In this case, for more than two time points, it is necessary to choose a time point for the subject-specific template, and this time point is generally the average (or median) of the observed time points. The momentum maps (from the template to all the time points) can then be compared in the template reference space only. Diffeomorphic transform is the exponential map of nSVF,  $v$ , and it is a time independent vector that induces diffeomorphic mapping  $\phi$ . Let us consider pairs of points in the image domain  $x_0, x_t \in \Omega$ ,  $t \in \mathbb{R}_+$ , such that  $x_t = \phi_t(x_0)$ . Here  $\phi$  is parametrized by time  $t$  as  $\frac{dx}{dt} = v(x)$ ,  $x(0) = x_0$ ,  $\phi_t(x_0) = x_t$ . The vector field is found as  $\frac{\partial \phi_t(x)}{\partial t} = v(x)$ . The inverse mapping is found by integrating  $-v$ , i.e. for  $y_0, y_t \in \Omega$ ,  $\frac{dy}{dt} = -v(y)$ ,  $y(0) = y_0$ ,  $\psi_t(y_0) = y_t$ . We suppose that the two input images are

**Algorithm 1** Diffeomorphic Registration

- Require:** A static image,  $Fxd$ , and a moving image,  $Mvg$ , such that  $\Omega \rightarrow \Gamma$ , where  $\Omega \subseteq \mathbb{R}^N$ ,  $\Gamma \subseteq \mathbb{R}$
- Ensure:** Determine the optimal transform  $T(x)$  minimizing the difference between  $Fxd$  and  $Mvg$
- 1: Seek a bijective mapping  $\phi : \Omega \rightarrow \Omega$ :  $Fxd \circ \phi$  to improve the similarity with  $Mvg$  and  $Mvg \circ \phi^{-1}$  improves similarity to  $Fxd$  under  $En(\phi)$ ,  $\phi$  being the diffeomorphic mapping
  - 2: The displacement field,  $u$ , is initialized
  - 3: A new symmetric function,  $En(l, \phi)$  is calculated using spatial transform parameter  $l$
  - 4: The energy functional in the displacement field,  $En(u)$ , is calculated
  - 5: Parametrize the spectral features  $\phi$  by time,  $t$ , as  $\frac{dx}{dt} = v(x)$ ,  $x(0) = x_0$ ,  $\phi_t(x_0) = x_t$
  - 6: The driving force is calculated and the velocity field is updated
  - 7: The updates in the velocity field during registering process are computed with spectral correspondence
  - 8: The deformation field is regulated
  - 9: Exponential mapping of deformation is obtained by diffeomorphic transform
  - 10: Similarity measurement function  $En$  is calculated and it is solved to judge the convergence
  - 11: Pairwise registration is performed

**TABLE 1.** Comparative performance of CT/CT registration with other techniques.

Method	MSE	NCC	SS	MI	FSIM	MAE
Lombaert et al. [38]	4.9043	0.9212	0.9288	0.567	0.9632	2.56 ± 2.89
Sureeat et al. [31]	5.4932	0.9193	0.9085	0.543	0.9556	2.76 ± 2.79
Pai et al. [30]	4.6987	0.9306	0.9223	0.608	0.9689	2.29 ± 2.52
Blendowski et al. [64]	5.0907	0.9206	0.9103	0.588	0.9577	2.56 ± 2.50
Shuo et al. [39]	4.8913	0.9336	0.9265	0.630	0.9721	2.09 ± 2.39
Darkner et al. [37]	4.7809	0.9379	0.9288	0.642	0.9751	2.12 ± 2.40
<b>Proposed method</b>	<b>1.3136</b>	<b>0.9962</b>	<b>0.9897</b>	<b>0.883</b>	<b>0.9922</b>	<b>1.52 ± 2.09</b>

affine registered using conditional mutual information [48], i.e.  $C(Fxd \circ \phi, Mvg) + C(Mvg \circ \phi^{-1}, Fxd)$ .

The optimal registration is found by minimizing (2) accommodating the conditional mutual information ( $C$ ) with respect to deformation.

$$\frac{\partial En}{\partial \phi} = \frac{\partial C}{\partial u} \bigg|_{u=Fxd \circ \phi} \frac{\partial Fxd}{\partial x} \bigg|_{x=\phi} + \frac{\partial Reg}{\partial \zeta} \bigg|_{\zeta=\phi} + \left( \frac{\partial C}{\partial u} \bigg|_{u=Mvg \circ \phi^{-1}} \frac{\partial Mvg}{\partial x} \bigg|_{x=\phi^{-1}} + \frac{\partial Reg}{\partial \zeta} \bigg|_{\zeta=\phi^{-1}} \right) \frac{\partial \phi^{-1}}{\partial \phi}$$

The numerical approximate is  $x_t = \phi(x_{t-1}) + f(v, x_{t-1}, \Delta t)$ . The convergence condition is continuously monitored until  $E(n) - E(n-1) < threshold$ . For this, we use mid-point rule:

$$En(\phi) \approx \Delta \phi En(\phi_1) + \Delta \phi En(\phi_2) + \Delta \phi En(\phi_3) + \dots + \Delta \phi En(\phi_n) \quad (4)$$

where  $\phi_i$  are the diffeomorphisms and  $i = 1 \dots n$ .

3) SUMMARY OF THE PROPOSED METHOD

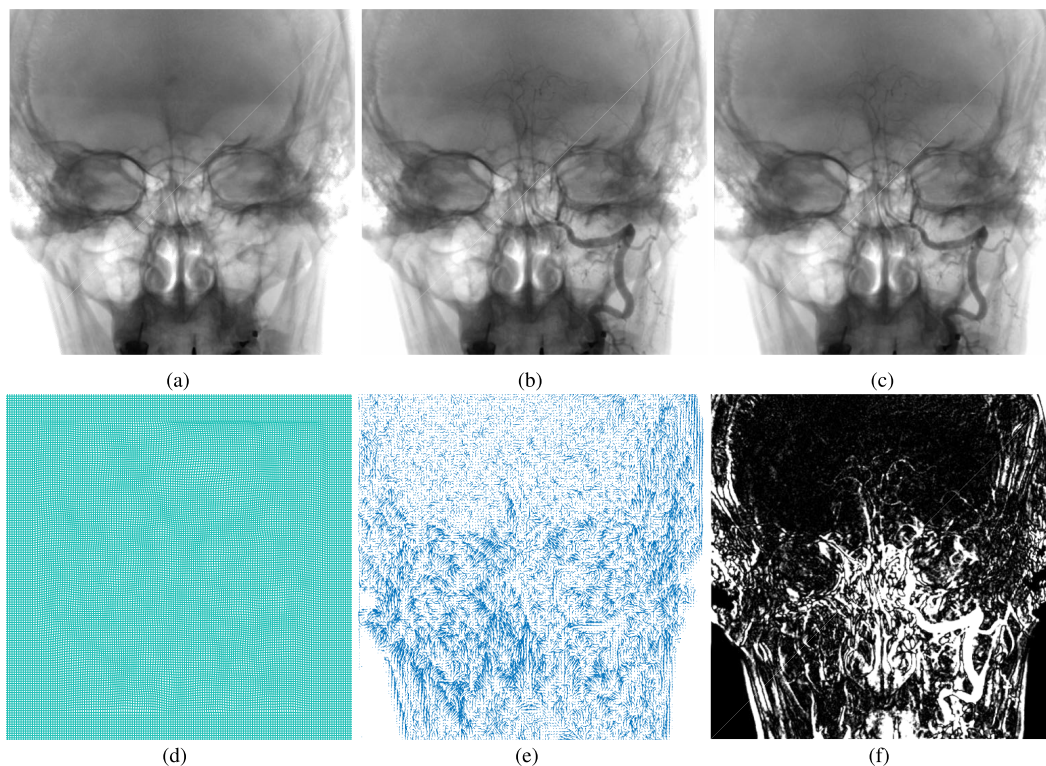
The key steps in the algorithm are summarized below (in Algorithm 1): The steps after 2 are iterative in nature and it

may be noted that the updates convergence rate is a measure that defines the efficacy of a diffeomorphic registration method; the denser is the convergence the faster is the registration.

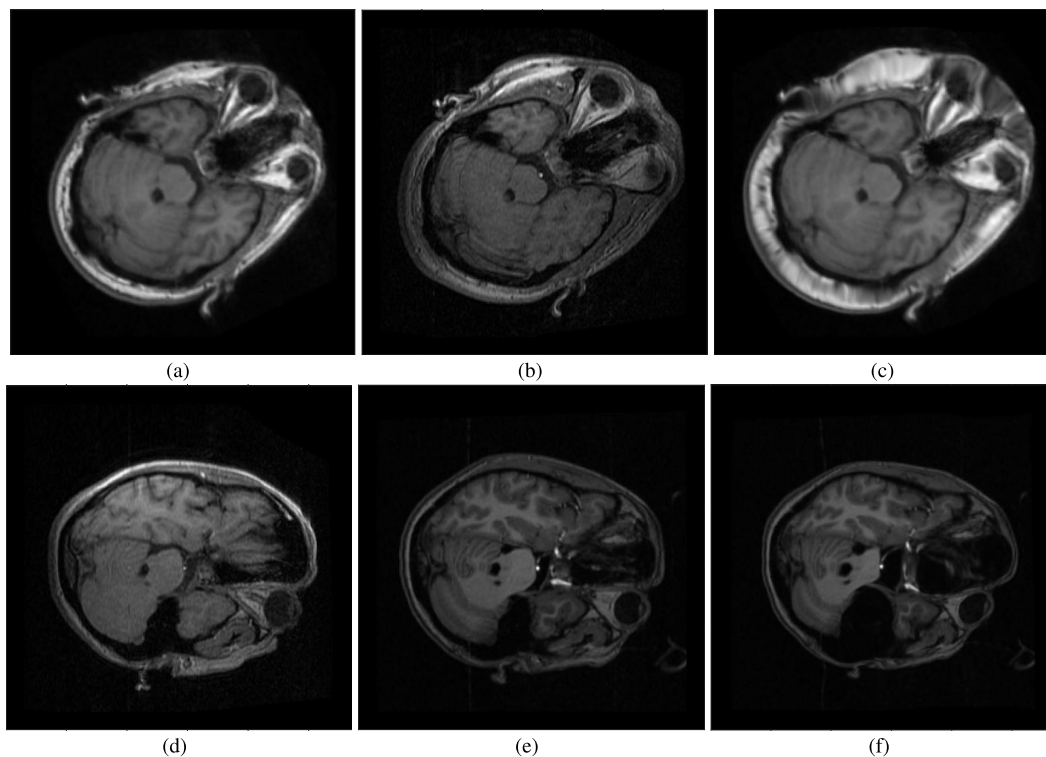
III. RESULTS

The proposed method is tested on the datasets obtained from Hamad Medical Corporation in Qatar, [43], and [44]. The data include brain aneurysm 3DRA data, brain tumor MR/CT data, and liver MR/CT data [47]. We have tested the algorithm on the images from same modality and cross-modalities as well. The results of registration processes are provided in Fig. 3, 4, 5, and 7. It may be observed that the proposed method has updates (indicated with the arrows) have faster convergence indicating a global scope.

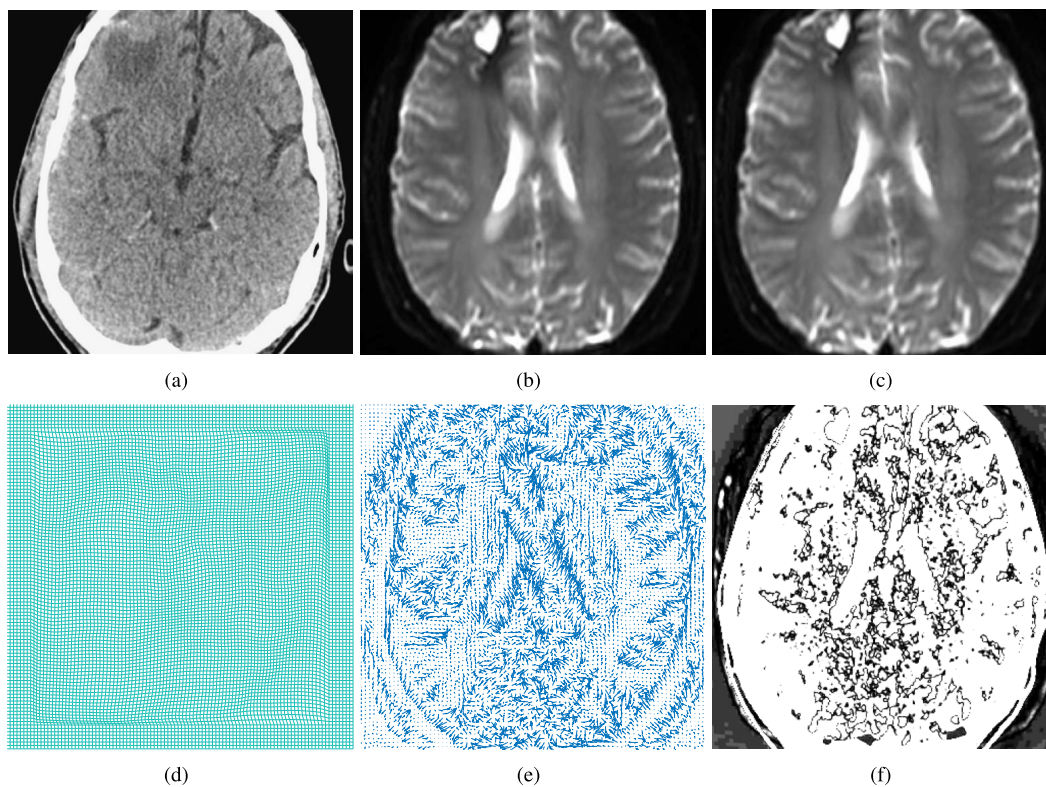
Fig. 3 provides the results when tested on brain aneurysm images. The reference image includes the aneurysm vessels that appear gradually, when the contrast agent is injected in the cerebral vessels, therefore, the two images are at different time instants. Similar is the case in Fig. 4. Fig. 5 and 6 provide results when tested on cross modalities, CT and MR. Fig. 7 provides the results of brain MR images but with deformations on moving image. We too have measured the similarities in terms of accuracy and variances as provided in Fig. 8. The algorithm has been implemented on MATLAB R2017b running on a workstation



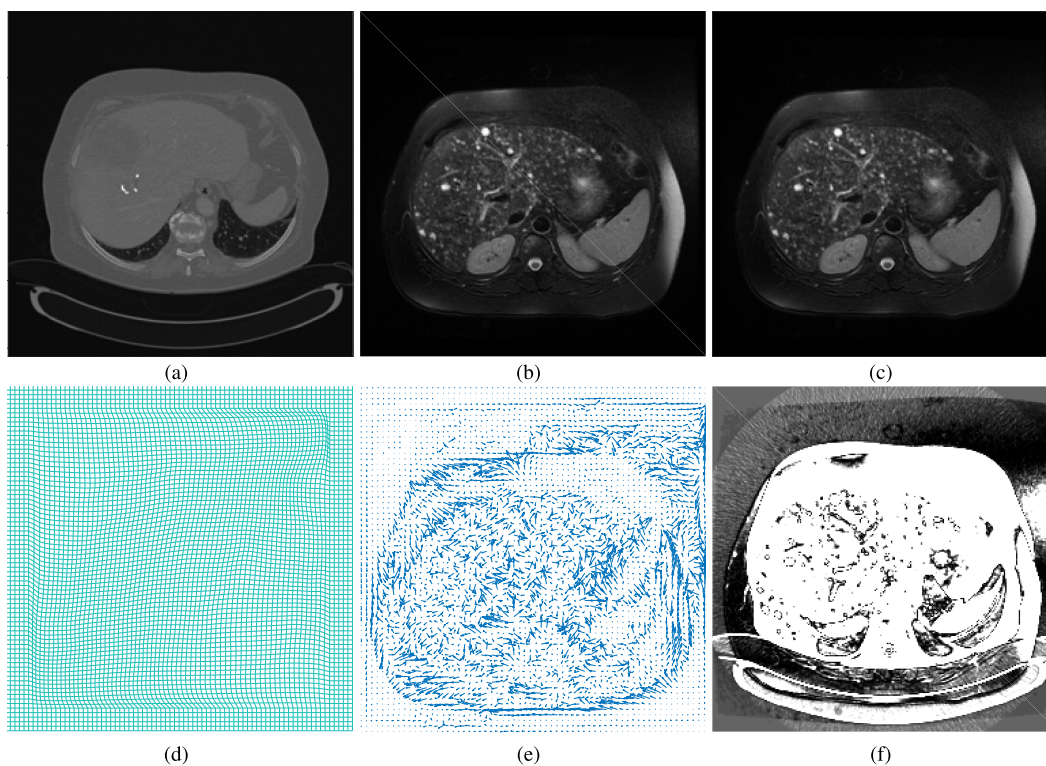
**FIGURE 3.** Same modal registration. (a) Moving 3DRA image with all cerebral vessels. (b) Reference 3DRA image with cerebral aneurysm after injecting contrast agent. (c) Registered image. (d) Deformation field image. (e) Updates in the velocity field during registering process. (f) Difference image.



**FIGURE 4.** Same modal registration. (a, d) Reference brain MR image. (b, e) Moving brain MR image. (c, f) Registered image.



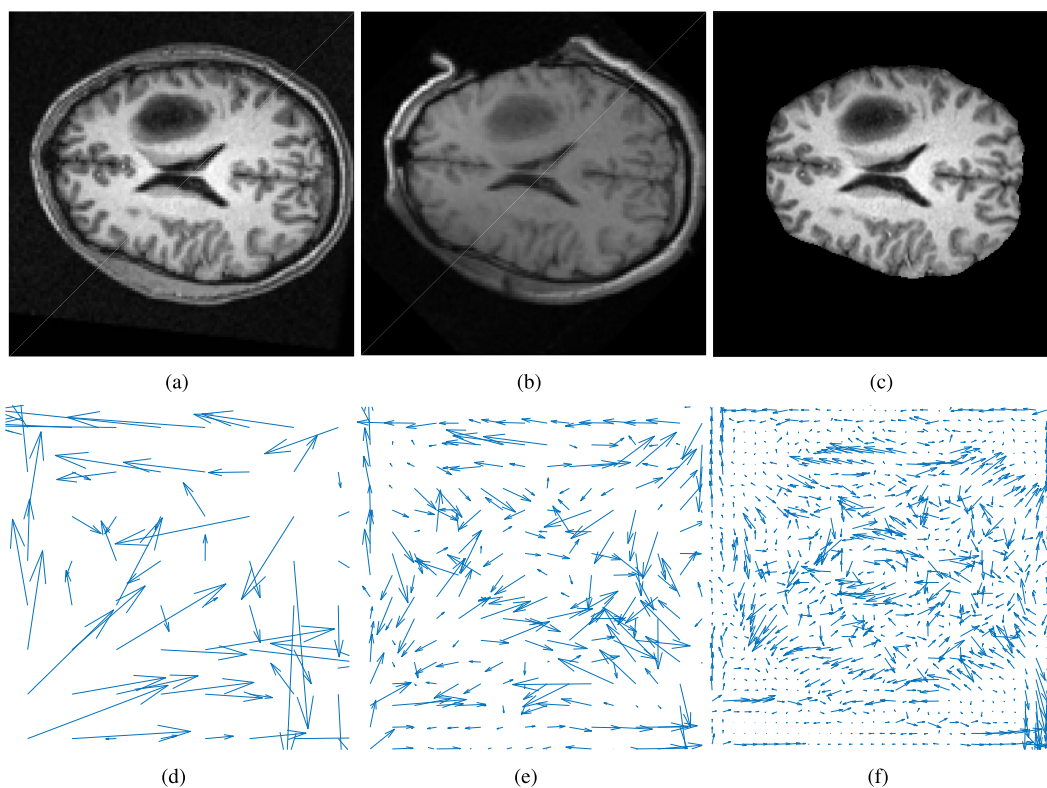
**FIGURE 5.** Multi-modal registration. (a) Moving brain CT image. (b) Reference brain MR image with tumor. (c) Registered image. (d) Deformation field image. (e) Updates in the velocity field during registering process. (f) Difference image.



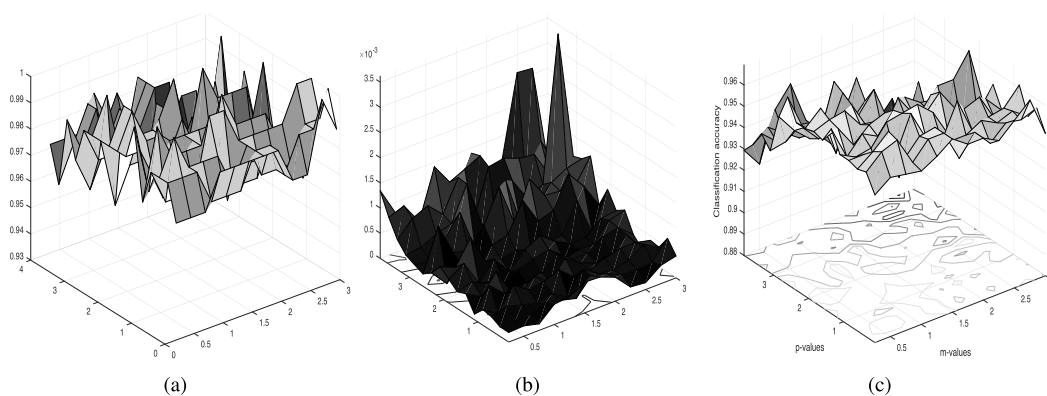
**FIGURE 6.** Multit-modal registration. (a) Moving liver CT image. (b) Reference liver MR image with tumor. (c) Registered image. (d) Deformation field image. (e) Updates in the velocity field during registering process. (f) Difference image.

**TABLE 2.** Comparative performance of 3DRA/3DRA registration with other techniques.

Method	MSE	NCC	SS	MI	FSIM	MAE
Lombaert et al. [38]	4.9855	0.9108	0.9054	0.558	0.9567	2.57 ± 2.36
Sureeat et al. [31]	5.8439	0.9082	0.8666	0.538	0.9349	2.81 ± 2.22
Pai et al. [30]	4.7582	0.9215	0.8872	0.598	0.9676	2.30 ± 2.44
Blendowski et al. [64]	5.3843	0.9101	0.8709	0.577	0.9494	2.57 ± 2.36
Shuo et al. [39]	4.8255	0.9227	0.8993	0.625	0.9673	2.10 ± 2.35
Darkner et al. [37]	4.8011	0.9292	0.9165	0.638	0.9689	2.16 ± 2.39
<b>Proposed method</b>	<b>1.3231</b>	<b>0.9820</b>	<b>0.9779</b>	<b>0.872</b>	<b>0.9813</b>	<b>1.54 ± 2.10</b>



**FIGURE 7.** Deformable same-modal image registration. (a) Reference brain MR image. (b) Moving brain MR image with missing information. (c) Registered image. (d-f) Updates in the velocity field during registering process.



**FIGURE 8.** Similarity measurements. (a) Maximum accuracies. (b) Variances. (c) Mean classification accuracies.



**TABLE 3. Comparative performance of MR/MR registration with other techniques.**

Method	MSE	NCC	SS	MI	FSIM	MAE
Lombaert et al. [38]	5.3812	0.8891	0.9088	0.540	0.9159	2.70 ± 2.20
Sureeat et al. [31]	5.8302	0.8729	0.8634	0.529	0.8971	2.85 ± 2.11
Pai et al. [30]	4.9420	0.8907	0.8865	0.591	0.9279	2.35 ± 2.17
Blendowski et al. [64]	5.4421	0.8829	0.8749	0.567	0.9033	2.59 ± 2.22
Shuo et al. [39]	5.2281	0.8923	0.8956	0.629	0.9387	2.18 ± 2.09
Darkner et al. [37]	5.0405	0.8925	0.9190	0.640	0.9493	2.20 ± 2.13
<b>Proposed method</b>	<b>1.7893</b>	<b>0.9511</b>	<b>0.9501</b>	<b>0.843</b>	<b>0.9633</b>	<b>1.60 ± 2.05</b>

**TABLE 4. Comparative performance of CT/MR registration with other techniques.**

Method	MSE	NCC	SS	MI	FSIM	MAE
Lombaert et al. [38]	6.2191	0.8796	0.8709	0.526	0.8726	2.78 ± 2.35
Sureeat et al. [31]	6.6989	0.8690	0.8328	0.502	0.8579	2.94 ± 2.05
Pai et al. [30]	5.3204	0.8811	0.8587	0.567	0.8822	2.45 ± 2.21
Blendowski et al. [64]	6.4188	0.8728	0.8466	0.526	0.8667	2.64 ± 2.32
Shuo et al. [39]	5.8290	0.8812	0.8652	0.557	0.8939	2.28 ± 2.18
Darkner et al. [37]	5.6113	0.8853	0.8888	0.568	0.9033	2.30 ± 2.33
<b>Proposed method</b>	<b>1.9895</b>	<b>0.9399</b>	<b>0.9287</b>	<b>0.812</b>	<b>0.9335</b>	<b>1.80 ± 1.95</b>

**TABLE 5. Comparative performance of registration accuracy with DL-based techniques.**

Method	MSE	NCC	SS	MI	FSIM	MAE
SyN	3.2394	0.9355	0.9231	0.612	0.9511	2.79 ± 2.12
LT-Net	3.0342	0.9422	0.9288	0.683	0.9534	2.44 ± 2.08
VoxelMorph	1.8701	0.9807	0.9802	0.862	0.9812	1.72 ± 2.10
<b>Proposed method</b>	<b>1.3136</b>	<b>0.9962</b>	<b>0.9897</b>	<b>0.883</b>	<b>0.9922</b>	<b>1.52 ± 2.09</b>

with 16 GB RAM and 2.8 GHz Intel processor; the average time to perform registration on a data with approximately 80 slices is little more than 1 minute that is quite reasonable from clinical perspective. We have also validated the method quantitatively. We have compared our method with various other diffeomorphic and non-diffeomorphic methods such as [31], [32], [39], [38], [40], and [65], using some popular measures such as mean square error (MSE), normalized cross-correlation (NCC), structural similarity (SS), mutual information (MI), feature similarity index (FSIM), and mean absolute error (MSE) [51]. The results of CT/CT, 3DRA/3DRA, MR/MR, and CT/MR are provided in Table 1, 2, 3, and 4, respectively. The values of MSE, NCC, SS, MI, FSIM, and MAE are found as 1.3136, 0.9962, 0.9897, 0.883, 0.9922, and 1.52 ± 2.09, respectively in CT/CT registration; for 3DRA/3DRA registration, the measures are found as: 1.3231, 0.9820, 0.9779, 0.872, 0.9813, and 1.54 ± 2.10, respectively; for MR/MR registration, they are 1.7893, 0.9511, 0.9501, 0.843, 0.9633, and 1.60 ± 2.05, respectively; for CT/MR registration, the measures are: 1.9895, 0.9399, 0.9287, 0.812, 0.9335, 1.80 ± 1.95, respectively. Thus, both the qualitative and quantitative results indicate that the proposed method is quite promising. Additionally, we have compared (in Table 5) the proposed method with

some popular DL-based methods, including Voxel-Morph (VM) [66], LT-Net [65], and Symmetric Normalization (SyN) [34]. We have selected these methods because they have been regularly preferred by the research fraternity for comparison purpose. Among these, Voxel-Morph is probably the most famous methods in recent years. The results show that the proposed method fairly performs as compared to the DL-based methods although the margin is not significant.

#### IV. DISCUSSION

From the Table 1, 2, 3, and 4, this can well be observed that the registration performance on CT/CT registration is the best among the other imaging modalities. The energy function plays an important role in this registration process. Therefore, we have investigated the effect of  $l$  after its introduction in (2) by subtracting (1) from (2),

$$\begin{aligned}
 & E_n(l, \phi) - E_n(\phi) \\
 &= [ \| (Fxd - Mvg \circ l) \|^2 + \frac{1}{\lambda_{un}^2} Disc(l, \phi)^2 ] \\
 & - [ \frac{1}{2 |\Omega_P|} \sum_{P \in \Omega_P} |Fxd(p) - Mvg(\phi(p))| ] \quad (5)
 \end{aligned}$$

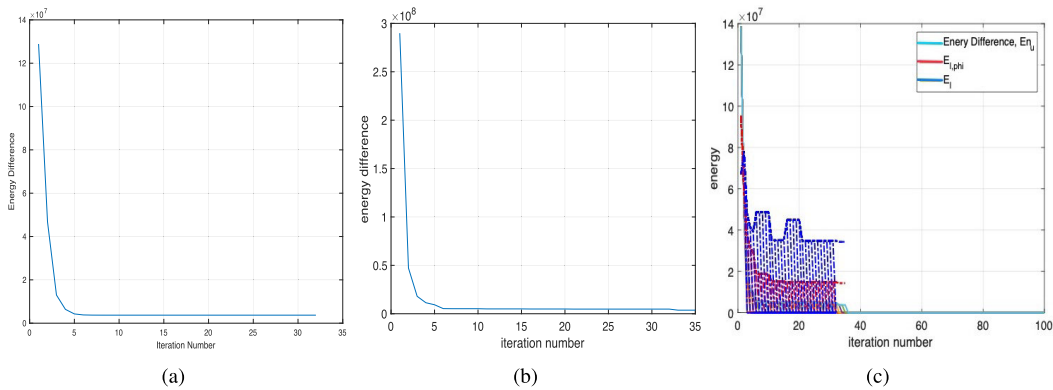


FIGURE 9. (a) Energy difference, (5). (b) Energy functional defined in (3). (c) All the energy functionals.

In order to have a decent comparison, we have plotted the difference of the two energy functionalities and their difference (5). Also, we have plotted the energy functionality defined in (3) and the difference to assess them fairly. All of these figures are provided in Fig. 9. We have found that the energy function defined in (3) converges appropriately reflecting its significance in image registration.

## V. CONCLUSION

In this paper, we have presented a non-rigid registration method that is based on diffeomorphic mapping. The results are promising with respect to large or small deformations; furthermore, it is not domain specific. The image gradients have little or no effect on the registration outputs. In future, we intend to test this method on large cross-modal platform with very large deformations.

## APPENDIX REGISTRATION EVALUATION MEASURES

In this section, some of the measures that evaluate the proposed registration method are included.

### A. MUTUAL INFORMATION

Mutual information (MI) is defined as [52]:

$$MI(X, Y) = IE(X) + IE(Y) - IE(X, Y) \quad (6)$$

where  $IE(X)$  and  $IE(Y)$  denote the information entropy of reference image  $X$  and float image  $Y$ , respectively.  $IE(X, Y)$  is the joint entropy of the two images.

### B. MEAN ABSOLUTE ERROR (MAE)

The mean absolute error is calculated over the neighborhood of the landmarks. The MAE of the real registration error  $RR_i$  and the estimated one  $\widehat{RR}_i$  is calculated by [53]:

$$MAE = \frac{1}{N} \sum_{i=1}^N |\widehat{RR}_i - RR_i| \quad (7)$$

where  $N$  is total number of pixels.

### C. FEATURE SIMILARITY INDEX

The feature similarity index (FSIM) is a similarity measure between two images  $X$  and  $Y$  is calculated as [55]:

$$FSIM = \frac{\sum_{x \in \Omega} S_L(x) \cdot PC_m(x)}{\sum_{x \in \Omega} PC_m(x)} \quad (8)$$

$\Omega$  means the whole image spatial domain. Here  $S_L(x)$  determines the similarity between  $X(x)$  and  $Y(x)$ . The maximum phase congruence  $PC_m(x)$  weighs the importance of  $S_L(x)$ .

### ACKNOWLEDGMENT

The findings herein reflect the work, and are solely the responsibility of the authors.

### REFERENCES

- [1] S. P. Dakua, "Towards left ventricle segmentation from magnetic resonance images," *IEEE Sensors J.*, vol. 17, no. 18, pp. 5971–5981, Sep. 2017.
- [2] S. P. Dakua, "Performance divergence with data discrepancy: A review," *Artif. Intell. Rev.*, vol. 40, pp. 429–555, Dec. 2011.
- [3] J. Müller, J. Müller, F. Chen, R. Tetzlaff, J. Müller, E. Böhl, M. Kirsch, and C. Schnabel, "Registration and fusion of thermographic and visual-light images in neurosurgery," *IEEE Trans. Biomed. Circuits Syst.*, vol. 12, no. 6, pp. 1313–1321, Dec. 2018.
- [4] F. Commandeur, A. Simon, R. Mathieu, M. Nassef, J. D. O. Arango, Y. Rolland, P. Haigron, R. de Crevoisier, and O. Acosta, "MRI to CT prostate registration for improved targeting in cancer external beam radiotherapy," *IEEE J. Biomed. Health Informat.*, vol. 21, no. 4, pp. 1015–1026, Jul. 2017.
- [5] Q. Li, R. Song, X. Ma, and X. Liu, "A robust registration algorithm for image-guided surgical robot," *IEEE Access*, vol. 6, pp. 42950–42960, 2018.
- [6] R. Kechichian, S. Valette, and M. Desvignes, "Automatic multiorgan segmentation via multiscale registration and graph cut," *IEEE Trans. Med. Imag.*, vol. 37, no. 12, pp. 2739–2749, Dec. 2018.
- [7] S. P. Dakua, J. Abinshed, A. Zakaria, S. Balakrishnan, G. Younes, N. Navkar, A. Al-Ansari, X. Zhai, F. Bensaali, and A. Amira, "Moving object tracking in clinical scenarios: Application to cardiac surgery and cerebral aneurysm clipping," *Int. J. Comput. Assist. Radiol. Surg.*, vol. 14, no. 12, pp. 2165–2176, Dec. 2019.
- [8] M. A. Viergever, J. B. A. Maintz, S. Klein, K. Murphy, M. Staring, and J. P. W. Pluim, "A survey of medical image registration—Under review," *Med. Image Anal.*, vol. 33, pp. 140–144, Oct. 2016.
- [9] S. Matl, R. Brosig, M. Baust, N. Navab, and S. Demirci, "Vascular image registration techniques: A living review," *Med. Image Anal.*, vol. 35, pp. 1–17, Jan. 2017.

- [10] I. J. A. Simpson, M. J. Cardoso, M. Modat, D. M. Cash, M. W. Woolrich, J. L. R. Andersson, J. A. Schnabel, and S. Ourselin, "Probabilistic non-linear registration with spatially adaptive regularisation," *Med. Image Anal.*, vol. 26, pp. 203–216, Dec. 2015.
- [11] J. Lotz, J. Olesch, B. Müller, T. Polzin, P. Galuschka, J. M. Lotz, S. Heldmann, H. Laue, M. Gonzalez-Vallinas, A. Warth, B. Lahrmann, N. Grabe, O. Sedlaczek, K. Breuhahn, and J. Modersitzki, "Patch-based nonlinear image registration for gigapixel whole slide images," *IEEE Trans. Biomed. Eng.*, vol. 63, no. 9, pp. 1812–1819, Sep. 2016.
- [12] J. Wang, R. Schaffert, A. Borsdorf, B. Heigl, X. Huang, J. Hornegger, and A. Maier, "Dynamic 2-D/3-D rigid registration framework using point-to-plane correspondence model," *IEEE Trans. Med. Imag.*, vol. 36, no. 9, pp. 1939–1954, Sep. 2017.
- [13] Y. Li, C. Chen, F. Yang, and J. Huang, "Hierarchical sparse representation for robust image registration," *IEEE Trans. Pattern Anal. Mach. Intell.*, vol. 40, no. 9, pp. 2151–2164, Sep. 2018.
- [14] M. Polfliet, S. Klein, W. Huizinga, M. M. Paulides, W. J. Niessen, and J. Vandemeulebroucke, "Intrasubject multimodal groupwise registration with the conditional template entropy," *Med. Image Anal.*, vol. 46, pp. 15–25, May 2018.
- [15] A. Turco, O. Gheysens, J. Nuyts, J. Duchenne, J. U. Voigt, P. Claus, and K. Vunckx, "Impact of CT-based attenuation correction on the registration between dual-gated cardiac PET and high-resolution CT," *IEEE Trans. Nucl. Sci.*, vol. 63, no. 1, pp. 180–192, Feb. 2016.
- [16] D. Pilutti, M. Strumia, M. Büchert, and S. Hadjidemetriou, "Non-parametric Bayesian registration (NParBR) of body tumors in DCE-MRI data," *IEEE Trans. Med. Imag.*, vol. 35, no. 4, pp. 1025–1035, Apr. 2016.
- [17] G. Samei, O. Goksel, J. Lobo, O. Mohareri, P. Black, R. Rohling, and S. Salcudean, "Real-time FEM-based registration of 3-D to 2.5-D transrectal ultrasound images," *IEEE Trans. Med. Imag.*, vol. 37, no. 8, pp. 1877–1886, Aug. 2018.
- [18] X. Cao, J. Yang, Y. Gao, Q. Wang, and D. Shen, "Region-adaptive deformable registration of CT/MRI pelvic images via learning-based image synthesis," *IEEE Trans. Image Process.*, vol. 27, no. 7, pp. 3500–3512, Jul. 2018.
- [19] P. Xu, C. Chen, X. Wang, W. Li, and J. Sun, "ROI-based intraoperative MR-CT registration for image-guided multimode tumor ablation therapy in hepatic malignant tumors," *IEEE Access*, vol. 8, pp. 13613–13619, 2020.
- [20] Y. Zhou, Q. Feng, Y. Sun, W. Yang, Z. Lu, M. Huang, L. Lu, Y. Zhang, Y. Feng, and W. Chen, "Correlation-weighted sparse representation for robust liver DCE-MRI decomposition registration," *IEEE Trans. Med. Imag.*, vol. 38, no. 10, pp. 2352–2363, Oct. 2019.
- [21] W. Huang, H. Yang, X. Liu, C. Li, I. Zhang, R. Wang, H. Zheng, and S. Wang, "A coarse-to-fine deformable transformation framework for unsupervised multi-contrast MR image registration with dual consistency constraint," *IEEE Trans. Med. Imag.*, vol. 40, no. 10, pp. 2589–2599, Oct. 2021.
- [22] L. Hansen and M. P. Heinrich, "GraphRegNet: Deep graph regularisation networks on sparse keypoints for dense registration of 3D lung CTs," *IEEE Trans. Med. Imag.*, vol. 40, no. 9, pp. 2246–2257, Sep. 2021.
- [23] M. Grimm, J. Esteban, M. Unberath, and N. Navab, "Pose-dependent weights and domain randomization for fully automatic X-ray to CT registration," *IEEE Trans. Med. Imag.*, vol. 40, no. 9, pp. 2221–2232, Sep. 2021.
- [24] H. Yu, H. Jiang, X. Zhou, T. Hara, Y.-D. Yao, and H. Fujita, "Unsupervised 3D PET-CT image registration method using a metabolic constraint function and a multi-domain similarity measure," *IEEE Access*, vol. 8, pp. 63077–63089, 2020.
- [25] T. Fechter and D. Baltas, "One-shot learning for deformable medical image registration and periodic motion tracking," *IEEE Trans. Med. Imag.*, vol. 39, no. 7, pp. 2506–2517, Jul. 2020.
- [26] S. Guan, C. Meng, Y. Xie, Q. Wang, K. Sun, and T. Wang, "Deformable cardiovascular image registration via multi-channel convolutional neural network," *IEEE Access*, vol. 7, pp. 17524–17534, 2019.
- [27] Y. Hu, E. Gibson, H. U. Ahmed, C. M. Moore, M. Emberton, and D. C. Barratt, "Population-based prediction of subject-specific prostate deformation for MR-to-ultrasound image registration," *Med. Image Anal.*, vol. 26, no. 1, pp. 332–344, Dec. 2015.
- [28] Z. Li, D. Mahapatra, J. A. W. Tielbeek, J. Stoker, L. J. van Vliet, and F. M. Vos, "Image registration based on autocorrelation of local structure," *IEEE Trans. Med. Imag.*, vol. 35, no. 1, pp. 63–75, Jan. 2016.
- [29] T. Vercauteren, X. Pennec, A. Perchant, and N. Ayache, "Non-parametric diffeomorphic image registration with the demons algorithm," in *Proc. 10th Int. Conf. Med. Image Comput. Comput.-Assist. Intervent.*, 2007, pp. 319–326.
- [30] A. Pai, S. Sommer, L. Sorensen, S. Darkner, J. Spurring, and M. Nielsen, "Kernel bundle diffeomorphic image registration using stationary velocity fields and Wendland basis functions," *IEEE Trans. Med. Imag.*, vol. 35, no. 6, pp. 1369–1380, Jun. 2016.
- [31] S. Reaungamornrat, T. D. Silva, A. Uneri, S. Vogt, G. Kleinszig, A. J. Khanna, J.-P. Wolinsky, L. J. Prince, and H. J. Siewerdsen, "MIND demons: Symmetric diffeomorphic deformable registration of MR and CT for image-guided spine surgery," *IEEE Trans. Med. Imag.*, vol. 35, no. 11, pp. 2413–2424, Nov. 2016.
- [32] J. A. Collins, J. A. Weis, J. S. Heiselman, L. W. Clements, A. L. Simpson, W. R. Jarnagin, and M. I. Miga, "Improving registration robustness for image-guided liver surgery in a novel human-to-phantom data framework," *IEEE Trans. Med. Imag.*, vol. 36, no. 7, pp. 1502–1510, Jul. 2017.
- [33] W. Sun, W. J. Niessen, and S. Klein, "Randomly perturbed B-splines for nonrigid image registration," *IEEE Trans. Pattern Anal. Mach. Intell.*, vol. 39, no. 7, pp. 1401–1413, Jul. 2017.
- [34] B. B. Avants, C. L. Epstein, M. Grossman, and J. C. Gee, "Symmetric diffeomorphic image registration with cross-correlation: Evaluating automated labeling of elderly and neurodegenerative brain," *Med. Image Anal.*, vol. 12, no. 1, pp. 26–41, Feb. 2008.
- [35] F. Zhao, Z. Wu, F. Wang, W. Lin, S. Xia, D. Shen, L. Wang, and G. Li, "S3Reg: Superfast spherical surface registration based on deep learning," *IEEE Trans. Med. Imag.*, vol. 40, no. 8, pp. 1964–1976, Aug. 2021.
- [36] B. Chakraborty, Z. Liu, B. Heyde, J. Luo, and J. D'hooge, "2-D myocardial deformation imaging based on RF-based nonrigid image registration," *IEEE Trans. Ultrason., Ferroelectr., Freq. Control*, vol. 65, no. 6, pp. 1037–1047, Jun. 2018.
- [37] S. Darkner, A. Pai, M. G. Liprot, and J. Spurring, "Collocation for diffeomorphic deformations in medical image registration," *IEEE Trans. Pattern Anal. Mach. Intell.*, vol. 40, no. 7, pp. 1570–1583, Jul. 2018.
- [38] H. Lombaert, L. Grady, X. Pennec, N. Ayache, and F. Chieriet, "Spectral log-demons: Diffeomorphic image registration with very large deformations," *Int. J. Comput. Vis.*, vol. 107, no. 3, pp. 254–271, 2014.
- [39] S. Zhang, P. X. Liu, M. Zheng, and W. Shi, "A diffeomorphic unsupervised method for deformable soft tissue image registration," *Comput. Biol. Med.*, vol. 120, May 2020, Art. no. 103708, doi: 10.1016/j.compbiomed.2020.103708.
- [40] B. Qin, Z. Shen, Z. Fu, Z. Zhou, Y. Lv, and J. Bao, "Joint-saliency structure adaptive kernel regression with adaptive-scale kernels for deformable registration of challenging images," *IEEE Access*, vol. 6, pp. 330–343, 2018.
- [41] L. Zhang, B. Li, L. Tian, and W. Zhu, "LPPCO: A novel multimodal medical image registration using new feature descriptor based on the local phase and phase congruency of different orientations," *IEEE Access*, vol. 6, pp. 71976–71987, 2018.
- [42] C. Yang, Y. Liu, X. Jiang, Z. Zhang, L. Wei, T. Lai, and R. Chen, "Non-rigid point set registration via adaptive weighted objective function," *IEEE Access*, vol. 6, pp. 75947–75960, 2018.
- [43] S. Bakas, H. Akbari, A. Sotiras, M. Bilello, M. Rozycki, J. S. Kirby, J. B. Freymann, K. Farahani, and C. Davatzikos, "Advancing the cancer genome atlas glioma MRI collections with expert segmentation labels and radiomic features," *Sci. Data*, vol. 4, no. 1, Dec. 2017, Art. no. 170117.
- [44] J. P. Mugler, III, and J. R. Brookeman, "Three-dimensional magnetization-prepared rapid gradient-echo imaging," *Magn. Reson. Med.*, vol. 15, pp. 152–157, Jul. 1990.
- [45] R. Caruana, Y. Lou, J. Gehrke, P. Koch, M. Sturm, and N. Elhadad, "Intelligible models for HealthCare: Predicting pneumonia risk and hospital 30-day readmission," in *Proc. 21th ACM SIGKDD Int. Conf. Knowl. Discovery Data Mining*, Aug. 2015, pp. 1721–1730.
- [46] Y. Ming, P. Xu, H. Qu, and L. Ren, "Interpretable and steerable sequence learning via prototypes," in *Proc. 25th ACM SIGKDD Int. Conf. Knowl. Discovery Data Mining*, Anchorage, AK, USA, Jul. 2019, pp. 903–913.
- [47] S. P. Dakua, "Use of chaos concept in medical image segmentation," *Comput. Methods Biomechanics Biomed. Eng., Vis. Imag.*, vol. 1, no. 1, pp. 8–36, 2013.
- [48] D. Loeckx, P. Slagmolen, F. Maes, D. Vandermeulen, and P. Suetens, "Nonrigid image registration using conditional mutual information," *IEEE Trans. Med. Imag.*, vol. 29, no. 1, pp. 19–29, Jan. 2010.

- [49] B. B. Avants, N. J. Tustison, G. Song, P. A. Cook, A. Klein, and J. C. Gee, "A reproducible evaluation of ANTs similarity metric performance in brain image registration," *NeuroImage*, vol. 54, no. 3, pp. 2033–2044, 2011.
- [50] J. Rühaak, T. Polzin, S. Heldmann, J. A. I. Simpson, H. Handels, J. Modersitzki, and P. M. Heinrich, "Estimation of large motion in lung CT by integrating regularized keypoint correspondences into dense deformable registration," *IEEE Trans. Med. Imag.*, vol. 36, no. 8, pp. 1746–1757, Aug. 2017.
- [51] Z. Xu, P. C. Lee, P. M. Heinrich, M. Modat, D. Rueckert, S. Ourselin, G. R. Abramson, and A. B. Landman, "Evaluation of six registration methods for the human abdomen on clinically acquired CT," *IEEE Trans. Biomed. Eng.*, vol. 63, no. 8, pp. 1563–1572, Aug. 2016.
- [52] X. Cao and Q. Ruan, "A survey on evaluation methods for medical image registration," in *Proc. IEEE/ICME Int. Conf. Complex Med. Eng.*, Beijing, China, May 2007, pp. 718–721.
- [53] C. Spanakis, E. Mathioudakis, N. Kampanis, M. Tsiknakis, and K. Marias, "Machine-learning regression in evolutionary algorithms and image registration," *IET Image Process.*, vol. 13, no. 5, pp. 843–849, Apr. 2019.
- [54] M. P. Sampat, Z. Wang, S. Gupta, A. C. Bovik, and M. K. Markey, "Complex wavelet structural similarity: A new image similarity index," *IEEE Trans. Image Process.*, vol. 18, no. 11, pp. 2385–2401, Nov. 2009.
- [55] L. Zhang, L. Zhang, X. Mou, and D. Zhang, "FSIM: A feature similarity index for image quality assessment," *IEEE Trans. Image Process.*, vol. 20, no. 8, pp. 2378–2386, Aug. 2011.
- [56] Z. Chen, Z. Xu, W. Yi, X. Yang, W. Hou, M. Ding, and O. Granichin, "Real-time and multimodal brain slice-to-volume registration using CNN," *Expert Syst. Appl.*, vol. 133, pp. 86–96, Nov. 2019.
- [57] X. Zhu, M. Ding, T. Huang, X. Jin, and X. Zhang, "PCANet-based structural representation for nonrigid multimodal medical image registration," *Sensors*, vol. 18, no. 5, p. 1477, May 2018.
- [58] P. Cachier, X. Pennec, and N. Ayache, "Fast non rigid matching by gradient descent: Study and improvements of the 'demons' algorithm," INRIA, Rocquencourt, France, Tech. Rep. RR-3706, Jun. 1999.
- [59] P. Cachier and N. Ayache, "Isotropic energies, filters and splines for vector field regularization," *J. Math. Imag. Vis.*, vol. 20, no. 3, pp. 251–265, May 2004.
- [60] F. Zhu, J. Ren, M. Ding, and X. Zhang, "The spiking cortical model based structural representations for non-rigid multi-modal medical image registration," *J. Med. Imag. Health Informat.*, vol. 7, no. 5, pp. 1001–1004, Sep. 2017.
- [61] F. Zhu, M. Ding, and X. Zhang, "Self-similarity inspired local descriptor for non-rigid multi-modal image registration," *Inf. Sci.*, vol. 372, pp. 16–31, Dec. 2016.
- [62] F. Yang, M. Ding, X. Zhang, W. Hou, and C. Zhong, "Non-rigid multi-modal medical image registration by combining L-BFGS-B with cat swarm optimization," *Inf. Sci.*, vol. 316, pp. 440–456, Sep. 2015.
- [63] F. Yang, M. Ding, X. Zhang, Y. Wu, and J. Hu, "Two phase non-rigid multi-modal image registration using Weber local descriptor-based similarity metrics and normalized mutual information," *Sensors*, vol. 13, no. 6, pp. 7599–7617, Jun. 2013.
- [64] M. Blendowski, N. Bouteldja, and M. P. Heinrich, "Multimodal 3D medical image registration guided by shape encoder–decoder networks," *Int. J. Comput. Assist. Radiol. Surg.*, vol. 15, no. 2, pp. 269–276, Feb. 2020.
- [65] S. Wang, S. Cao, D. Wei, R. Wang, K. Ma, L. Wang, D. Meng, and Y. Zheng, "LT-Net: Label transfer by learning reversible voxel-wise correspondence for one-shot medical image segmentation," in *Proc. IEEE/CVF Conf. Comput. Vis. Pattern Recognit. (CVPR)*, Jun. 2020, pp. 9162–9171.
- [66] G. Balakrishnan, A. Zhao, M. R. Sabuncu, J. Guttag, and A. V. Dalca, "VoxelMorph: A learning framework for deformable medical image registration," *IEEE Trans. Med. Imag.*, vol. 38, no. 8, pp. 1788–1800, Aug. 2019.



**SNIGDHA MOHANTY** received the master's degree from the University College of Engineering (currently, Veer Surendra Sai University of Technology), Burla, India. She is currently pursuing the Ph.D. degree with KIIT University, Bhubaneswar, India, where she is a Research Scholar. Her research interests include medical image segmentation and registration.



**SARADA PRASAD DAKUA** (Member, IEEE) received the M.B.A. degree from the University of Leicester, U.K., and the Ph.D. degree from IIT Guwahati in medical image processing and analysis. He had spent over six years at the Qatar Robotic Surgery Centre, Qatar Science and Technology Park (Qatar Foundation) as a Research and Development Executive. He has more than 14 years of research experience in computer vision and image processing. He is working as a Senior Research Scientist with the Department of Surgery, Hamad Medical Corporation (HMC), since 2017. He is a certified PMP in his M.B.A. degree.

• • •